Image Cover Sheet

CLASSIFICATION	SYSTEM NUMBER
UNCLASSIFIED	502901

TITLE

A HYBRID SPLIT-STEP/FINITE-DIFFERENCE PE ALGORITHM FOR VARIABLE-DENSITY MEDIA

System Number:

Patron Number:

Requester:

Notes:

DSIS Use only:

Deliver to:

A hybrid split-step/finite-difference PE algorithm for variable-density media

David Yevick
Department of Electrical Engineering, Queen's University, Kingston, Ontario K7L 3N6, Canada

David J. Thomson
Defence Research Establishment Atlantic, Esquimalt Defence Research Detachment, CFB Esquimalt, PO Box 17000 STN FORCES, British Columbia V9A 7N2, Canada

(Received 23 January 1996; accepted for publication 2 October 1996)

Although variations in the density, ρ, are naturally incorporated into finite-difference parabolic equation (PE) solvers, split-step PE algorithms traditionally account for density changes by adding to the refractive index terms containing derivatives of ρ. As a consequence, geoacoustic density profiles that contain step discontinuities at layer interfaces must be smoothed appropriately before these extra terms can be evaluated. In this paper, a new hybrid method is proposed for treating density inhomogeneities in the split-step PE. This approach involves splitting the differential operator into density-independent and density-dependent components. While the former terms may be evaluated with the split-step Fourier technique, the influence of density changes is handled through a finite-difference procedure. Such an algorithm can be easily implemented in recently proposed hybrid split-step/finite-difference and split-step/Lanczos PE solvers. [J. Acoust. Soc. Am. **96**, 396–405 (1994)]. [S0001-4966(97)03302-X]

PACS numbers: 43.30.Bp [MBP]

INTRODUCTION

Both split-step and finite-difference marching algorithms are widely used to solve parabolic equations (PEs) that are derived from approximations to the exact, one-way wave equation of underwater sound propagation. However, while each numerical procedure is easily adapted to treat propagation in a constant-density ocean, the modifications needed to accommodate variable-density media differ for the two cases. In the finite-difference formalism, a so-called "homogeneous" procedure results if the density is taken to be uniform on both sides of a jump discontinuity (typically, the ocean bottom) and continuity conditions for both the pressure and particle velocity are imposed by appropriately modifying the equations describing the field in the vicinity of the interface.[1,2] Alternatively, in the "heterogeneous" procedure, a finite-difference approximation is applied directly to the relevant, density-dependent, transverse differential operator.[3–6] Neither of these procedures can be applied directly in the split-step Fourier algorithm. Instead, a change of variables is invoked to transfer the influence of density variations from the depth-dependent differential operator to the refractive index, allowing the separation of the propagator into a sum of a constant-coefficient, transverse derivative term and a position-space term which includes an effective index of refraction.[7,8] This term, however, contains density derivatives so that any jump discontinuities in the geoacoustic density profile must be smoothed by convolution with an appropriate analytic function.[6,9–12] In any given application, the accuracy of this approach is related to the width chosen for the smoothing function transition region, typically set to equal λ_0/π,[9] where λ_0 is an appropriate reference acoustic wavelength.

To avoid the above complications in the variable-density, split-step PE, we propose in this paper an alternative hybrid technique that does not rely on a smoothing parameter and that can be easily introduced into existing, widely used split-step codes.[13–15] In particular, we separate the effects of the nonuniform density by splitting the propagator into density-independent and density-dependent components. The former can be treated in the standard manner with the split-step scheme. The latter components, which appear as corrections to either the standard or wide-angle propagation operator, are instead implemented with the aid of finite-difference methods. Specifically, by applying the Crank–Nicolson procedure to the [1,1]-Padé approximant of the variable-density propagator, the correction term only gives rise to a single extra tridiagonal system of equations at each range step in addition to the computations associated with the split-step algorithm. The proposed formalism can be incorporated naturally into the hybrid split-step/finite difference and split-step/Lanczos procedures developed previously,[16] considerably extending their range of applicability.

The remainder of this paper is organized as follows. First, we introduce our new operator-splitting into standard and higher-order PE approximations that are amenable to the split-step algorithm. We then propose a finite-difference solution method for the variable-density component of the total propagator. We test this procedure for two shallow-water test cases which exhibit large density-dependent effects and present a comparison both with the traditional PE method using a smoothed density jump and with reference solutions computed using a wave number integration code. Finally, we discuss and summarize our theoretical and numerical results.

I. THEORETICAL METHOD

A. Fundamental equations

To construct the relevant one-way propagation equation for a medium with varying density $\rho(z)$, we consider a region $0<z<z_b$ between the surface ($z=0$) and bottom

($z=z_b$) of a stratified ocean with sound speed and absorption designated by $c(z)$ and $\alpha(z)$ respectively. We assume a uniform half-space in $z>z_b$ with values c_b, α_b and ρ_b. If changes in the pressure field $P(r,z,\phi,t)$ with respect to the azimuthal coordinate ϕ in a cylindrical coordinate system (r,ϕ,z) produced by a harmonic ($\omega=2\pi f$) point source located at $(r,z)=(0,z_s)$ are slow compared to the fluctuations in the (r,z)-plane, then P may be approximated along any radial by $P(r,z,t)=p(r,z)\exp(-i\omega t)$. For $r>0$, and for a density function which (locally) is solely dependent on the depth coordinate z, the complex pressure $p(r,z)$ then satisfies the two-dimensional scalar Helmholtz equation

$$\frac{1}{r}\frac{\partial}{\partial r}\left(r\frac{\partial p}{\partial r}\right)+\rho\frac{\partial}{\partial z}\left(\frac{1}{\rho}\frac{\partial p}{\partial z}\right)+k_0^2N^2p=0, \tag{1}$$

where $N(z)=n(z)+i\alpha(z)/k_0$, $n(z)=c_0/c(z)$ is the refractive index and $k_0=\omega/c_0$ is an arbitrary reference wave number. Then, if we define

$$\psi(r,z)=p(r,z)\exp(-ik_0r)\sqrt{k_0r} \tag{2}$$

we may describe outgoing propagating waves in the far-field ($k_0r\gg1$) by the "one-way" evolution equation[9,17]

$$\frac{\partial\psi}{\partial r}=ik_0(Q-1)\psi, \tag{3}$$

whose formal solution is given by

$$\psi(r+\Delta r,z)=\exp\{ik_0\Delta r(Q-1)\}\psi(r,z). \tag{4}$$

Here the quantity Q denotes the pseudo-differential operator

$$Q=\sqrt{N^2+k_0^{-2}\rho\frac{\partial}{\partial z}\left(\rho^{-1}\frac{\partial}{\partial z}\right)}. \tag{5}$$

Since the exact square-root operator Q is difficult to evaluate numerically, efficient computational schemes for implementing the exponential propagator in Eq. (4) are obtained from approximations to Q which lead to diagonally banded operators. While finite-difference representations for the full variable-density operator appearing in Eq. (4) can be developed in a straightforward way,[5,6] to handle density variations in the context of the split-step algorithm, it is instead customary to introduce the change of variable $\tilde{\psi}=\sqrt{\rho}\psi$.[7,8,12] Then, instead of Eq. (4), we obtain

$$\tilde{\psi}(r+\Delta r,z)=\exp\{ik_0\Delta r(\tilde{Q}-1)\}\tilde{\psi}(r,z). \tag{6}$$

where $\tilde{Q}$ is

$$\tilde{Q}=\sqrt{\tilde{N}^2+k_0^{-2}\frac{\partial^2}{\partial z^2}} \tag{7}$$

and $\tilde{N}$ is the "effective" index of refraction defined by

$$\tilde{N}^2=N^2+\frac{1}{2k_0^2}\sqrt{\rho}\frac{\partial}{\partial z}\left(\frac{1}{\rho\sqrt{\rho}}\frac{\partial\rho}{\partial z}\right). \tag{8}$$

As a result of the presence of derivatives of ρ in the expression for $\tilde{N}$, any step discontinuities contained in standard geoacoustic density profiles must first be smoothed appropriately. Thus, a discontinuous jump in density from ρ_1 to ρ_2 at the depth $z=\zeta$ is replaced by an analytic function of the form[9]

$$\rho(z)=\rho_1+\tfrac{1}{2}(\rho_2-\rho_1)\{1+\tanh[(z-\zeta)/L]\}, \tag{9}$$

where L defines the width of the transition region and is generally chosen such that $k_0L\approx2$. Multiple density jumps can be handled effectively using digital filter techniques based on Eq. (9).[11]

B. Propagator approximations

We now derive a split-step propagation procedure for variable density profiles based on Eq. (4) which does not require smoothing of the density profile. Our method is derived by extending the standard split-step method. That is, we first introduce the notation

$$\varepsilon=N^2-1, \tag{10}$$

$$\mu=\frac{1}{k_0^2}\frac{\partial^2}{\partial z^2}, \tag{11}$$

and

$$\gamma=-\frac{1}{k_0^2\rho}\frac{\partial\rho}{\partial z}\frac{\partial}{\partial z}, \tag{12}$$

and expand the right-hand side of Eq. (5) in the binomial series,

$$\begin{aligned}Q&=\sqrt{1+\varepsilon+\mu+\gamma}\\&=1+\sum_{j=1}^{\infty}\binom{\frac{1}{2}}{j}(\varepsilon+\mu+\gamma)^j\\&=1+\tfrac{1}{2}(\varepsilon+\mu+\gamma)-\tfrac{1}{8}(\varepsilon+\mu+\gamma)^2+\tfrac{1}{16}(\varepsilon+\mu+\gamma)^3\\&\quad+\cdots.\end{aligned} \tag{13}$$

If the norm of $N^2-1+k_0^{-2}\partial_{zz}-k_0^{-2}\rho^{-1}\rho_z\partial_z$ applied to the propagating field is sufficiently small, then the series equation (13) can be truncated after the second term to yield

$$Q_0=1+\tfrac{1}{2}(\varepsilon+\mu+\gamma). \tag{14}$$

This approximation leads to the standard, narrow-angle parabolic equation of underwater acoustics.[9,16,17] Substituting Eq. (14) into Eq. (4) yields the propagator

$$\exp\{\tfrac{1}{2}i\delta(\varepsilon+\mu+\gamma)\}\approx\underbrace{\exp\{\tfrac{1}{2}i\delta\gamma\}}_{\text{density}}\underbrace{\exp\{\tfrac{1}{2}i\delta\mu\}}_{\text{diffraction}}\underbrace{\exp\{\tfrac{1}{2}i\delta\varepsilon\}}_{\text{lens}}, \tag{15}$$

in which δ denotes $k_0\Delta r$. Because the individual operators defined in Eqs. (10)–(12) do not commute, replacing this exponential of the sum by the product of the exponentials is correct only to terms that are linear in Δr. For constant-density profiles ($\gamma=0$), the right-hand side of Eq. (15) reduces to a form that can be implemented directly by the split-step algorithm. In general, however, $\gamma\neq0$, and the evaluation of the density propagator requires special treatment. Following the hybrid solution approach of our previ-

ous work,[16] we propose to evaluate the lens and diffraction propagators using the split-step method while we apply a finite-difference technique to the density operator. It should be noted that if both the density and refractive index profiles contain discontinuities, it is essential to observe the ordering of the density, diffraction and lens operators as given on the right-hand side of Eq. (15). Otherwise, the large derivatives of the field generated by the lens operator will not be smoothed through subsequent diffraction and absorption in the diffraction step prior to application of the density operator. In this case, the derivative terms in the density operator will convert the high-frequency lens components into low-order modes, causing large errors in the propagating field.

We now demonstrate that our procedure can be simply extended to accommodate higher-order variable-density split-step PEs. Such equations incorporate additional terms of the binomial series in Eq. (13). For example, the one-term, rational-linear approximation Q_1, originally introduced by Claerbout[18]

$$Q_1=\frac{1+\frac{3}{4}(\varepsilon+\mu+\gamma)}{1+\frac{1}{4}(\varepsilon+\mu+\gamma)}=Q_0-\tfrac{1}{8}(\varepsilon+\mu+\gamma)^2+\cdots, \tag{16}$$

agrees with the first three terms of the series expansion of Q including the six cross terms involving the three operators ε, μ, and γ. Even when $\gamma=0$, the remaining cross-terms preclude the direct use of the split-step algorithm. The [1,1]-Padé approximant derived from this so-called rational-linear approximation, and from its n-term Padé series extension Q_n, can however be implemented easily using finite-difference techniques.[5,6,19]

Alternatively, retaining all terms in Eq. (13) that do *not* involve cross products of ε, μ, and γ leads to [6,16]

$$Q_1'=-2+\sqrt{1+\varepsilon}+\sqrt{1+\mu}+\sqrt{1+\gamma}. \tag{17}$$

Substituting Eq. (17) into Eq. (4) and neglecting terms of $O(\Delta r^2)$ yields

$$\begin{aligned}\exp\{i\delta(Q_1'-1)\}&=\exp\{i\delta(-3+\sqrt{1+\varepsilon}+\sqrt{1+\mu}+\sqrt{1+\gamma})\}\\&\approx\underbrace{\exp\{-i\delta+i\delta\sqrt{1+\gamma}\}}_{\text{density}}\underbrace{\exp\{-i\delta+i\delta\sqrt{1+\mu}\}}_{\text{diffraction}}\\&\quad\times\underbrace{\exp\{-i\delta+i\delta\sqrt{1+\varepsilon}\}}_{\text{lens}}.\end{aligned} \tag{18}$$

When $\gamma=0$, the above wide-angle, split-operator approximation to the propagator can again be implemented by the split-step Fourier algorithm.[6,20,21] For variable-density media, however, we can still use a hybrid solution procedure, where, in addition to the split-step operations, the separate density propagator is evaluated with finite-difference techniques, in much the same way as we have treated an analogous operator arising in electric field propagation.[22] Clearly, when the conditions underlying Eq. (14) are satisfied, the narrow-angle propagator in Eq. (15) can be obtained from the wide-angle propagator in Eq. (18) by expanding the exponentials. As before, to maintain numerical stability, the operator ordering given on the right-hand side of Eq. (18) should be preserved.

Following the approach used in Ref. 16, the split-operator approximation to Eq. (17) may be improved by successively introducing higher-order cross-terms containing Q, namely

$$Q_n'=Q_1'+\sum_{j=2}^{n}\binom{\frac{1}{2}}{j}[(\varepsilon+\mu+\gamma)^j-\varepsilon^j-\mu^j-\gamma^j]=Q_1'-\underbrace{\tfrac{1}{8}[(\varepsilon+\mu+\gamma)^2-\varepsilon^2-\mu^2-\gamma^2]+\tfrac{1}{16}[(\varepsilon+\mu+\gamma)^3-\varepsilon^3-\mu^3-\gamma^3]+\cdots}_{n-1\ \text{terms}}. \tag{19}$$

In practice, only the lowest-order contributions can be evaluated simply by finite-difference techniques. Higher-order corrections involving products of third and higher-order derivatives with spatially varying functions are more easily analyzed in the context of the Lanczos formalism.[16,23]

A specific hybrid form for the wide-angle, split-step PE derived from the variable-density operator Q_2' can be obtained by substituting Eq. (17) and Eq. (19) with $n=2$ into Eq. (4). The resulting propagator can be written

$$\begin{aligned}\exp\{i\delta(Q_2'-1)\}&=\exp\{i\delta(Q_1'-1)-\tfrac{1}{8}i\delta[\varepsilon(\mu+\gamma)+(\mu+\gamma)\varepsilon+\mu\gamma+\gamma\mu]\}\\&\approx\exp\{i\delta(Q_1'-1)\}\underbrace{\exp\{-\tfrac{1}{8}i\delta[\varepsilon(\mu+\gamma)+(\mu+\gamma)\varepsilon+\mu\gamma+\gamma\mu]\}}_{\text{cross-terms}}.\end{aligned} \tag{20}$$

The propagator containing Q_1' may then be generated using the hybrid split-step/finite-difference procedure suggested by Eq. (18). The remaining propagator in Eq. (20), which depends on the lowest-order cross-terms, can also be implemented by finite-difference methods. For $\gamma\neq0$, this hybrid procedure involving $\exp\{i\delta(Q_2'-1)\}$ thus requires two Padé approximant propagators in addition to the operations required by the split-step algorithm.

II. NUMERICAL IMPLEMENTATION

We now consider the computational aspects associated with the variable-density propagators introduced in the previous section. Beginning with Eq. (18), we recall that the first two propagators generated by the operator Q_1' can be evaluated with the split-step algorithm. In particular, the lens component, which depends on ε, may be applied through an element-by-element vector multiplication in z-space while the diffraction component, which depends on μ, is implemented similarly in k_z-space, the Fourier transform domain of z. In practice, these Fourier transforms (and their inverses) are carried out using the fast Fourier transform (FFT) algorithm, yielding[6,16,20,21,24]

$$\psi(r+\Delta r',z)\approx\exp\{i\delta(N-2)\}\cdot \mathrm{FFT}^{-1}[\exp\{i\delta\sqrt{1-k_z^2/k_0^2}\}\cdot \mathrm{FFT}[\psi(r,z)]]. \tag{21}$$

Here $r+\Delta r'$ is used to denote a density-independent state intermediate to r and $r+\Delta r$. When $\gamma\neq 0$, the third propagator, which depends on density through γ, can be handled by Padé approximant methods. Specifically, this component can be approximated by the unitary, z-space representation

$$\exp\{-i\delta+i\delta\sqrt{1+\gamma}\}\approx\frac{1+\frac{1}{4}(1+i\delta)\gamma}{1+\frac{1}{4}(1-i\delta)\gamma} \tag{22}$$

which generates the finite-difference system of equations

$$\{1+\tfrac{1}{4}(1-i\delta)\gamma\}\psi(r+\Delta r,z)=\{1+\tfrac{1}{4}(1+i\delta)\gamma\}\psi(r+\Delta r',z). \tag{23}$$

A suitable approximation for $\gamma\psi$ can be obtained from the heterogeneous finite-difference representation of the transverse derivative expression containing the variable ρ[6]

$$\mu'\psi(r,z)=\frac{\rho}{k_0^2}\frac{\partial}{\partial z}\left(\rho^{-1}\frac{\partial\psi(r,z)}{\partial z}\right)\approx\frac{\rho_-\psi(r,z-\Delta z)-\rho_0\psi(r,z)+\rho_+\psi(r,z+\Delta z)}{k_0^2\Delta z^2}, \tag{24}$$

where the variables

$$\rho_\pm=\frac{2\rho(r,z)}{\rho(r,z)+\rho(r,z\pm\Delta z)} \tag{25}$$

and

$$\rho_0=\rho_-+\rho_+ \tag{26}$$

have been introduced. When ρ is constant, Eq. (24) reduces to the standard second-order difference form for the operator μ. Since $\mu'\equiv\mu+\gamma$, a finite-difference approximation for $\gamma\psi$ can be obtained by forming

$$\gamma\psi(r,z)\equiv(\mu'-\mu)\psi(r,z)\approx[(\rho_--1)\psi(r,z-\Delta z)-(\rho_0-2)\psi(r,z)+(\rho_+-1)\psi(r,z+\Delta z)]/(k_0^2\Delta z^2). \tag{27}$$

TABLE I. Geoacoustic profile for the Bucker case.

Depth (m)	Sound speed (m s^{-1})	Density (g cm^{-3})	Attenuation dB λ^{-1}
0	1500	1.0	0.0
120	1498	1.0	0.0
240	1500	1.0	0.0
240	1505	2.1	0.0
1024	1505	2.1	0.0
2048	1505	2.1	0.5

The fourth exponential operator associated with Q_2' in Eq. (20) can be represented by the Padé approximant

$$\exp\{-\tfrac{1}{8}i\delta(\varepsilon\mu'+\mu'\varepsilon+\mu\gamma+\gamma\mu)\}\approx\frac{1-\frac{1}{16}i\delta(\varepsilon\mu'+\mu'\varepsilon+\mu\gamma+\gamma\mu)}{1+\frac{1}{16}i\delta(\varepsilon\mu'+\mu'\varepsilon+\mu\gamma+\gamma\mu)}. \tag{28}$$

If $\gamma=0$, the representation in Eq. (28) reduces to the same hybrid form that was introduced in Ref. 16, and thus leads to a tridiagonal system of equations. When $\gamma\neq 0$, however, the finite-difference evaluation of $\mu\gamma\psi$ and $\gamma\mu\psi$ involves the operator $\partial^3/\partial z^3$ which leads to a higher-order system. To circumvent this complication, we choose to neglect third-order contributions to the propagating field. From Eq. (24), we further observe that the terms involving $\varepsilon\mu'\psi$ and $\mu'\varepsilon\psi$ can be approximated by the finite-difference expressions

$$\varepsilon\mu'\psi(r,z)\approx\varepsilon(r,z)\frac{\rho_-\psi(r,z-\Delta z)-\rho_0\psi(r,z)+\rho_+\psi(r,z+\Delta z)}{k_0^2\Delta z^2} \tag{29}$$

and

$$\mu'\varepsilon\psi(r,z)\approx[\rho_-\varepsilon(r,z-\Delta z)\psi(r,z-\Delta z)-\rho_0\varepsilon(r,z)\psi(r,z)+\rho_+\varepsilon(r,z+\Delta z)\psi(r,z+\Delta z)]/(k_0^2\Delta z^2). \tag{30}$$

Substituting the above formulas into the Padé approximant of the operator for Eq. (28) and applying the Crank–Nicolson procedure leads to a tridiagonal system of equations.[6,25]

III. NUMERICAL RESULTS

In this section, we demonstrate our numerical implementation of the split-operator, variable-density procedure for two shallow-water propagation examples. In the first of these, attributed to Bucker and given in Table I, the geoacoustic profile contains jump discontinuities in both sound speed and density along the ocean bottom at $z=240$ m. This Bucker profile has previously been employed by a number of authors to establish the ability of their PE solvers to accommodate density variations.[1,2,11] Although the small ε-contrast results in only a small number of normal modes with real propagation wave numbers, the large γ-contrast yields a significant number of virtual modes close to the real

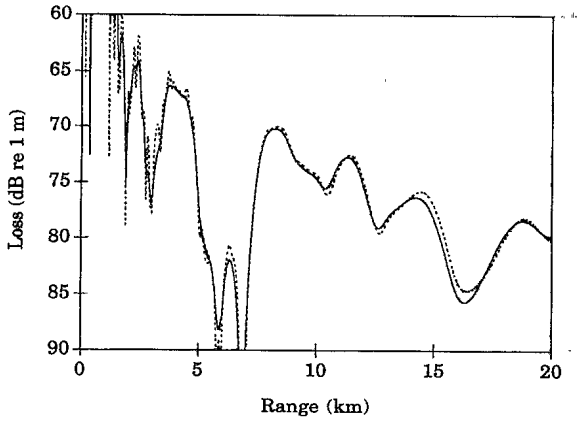

FIG. 1. Transmission loss versus range for the Bucker profile and a receiver depth of 90 m. Dashed line: SAFARI. Solid line: Split-step PE using $\tilde{Q}$ with $k_0L=2$.

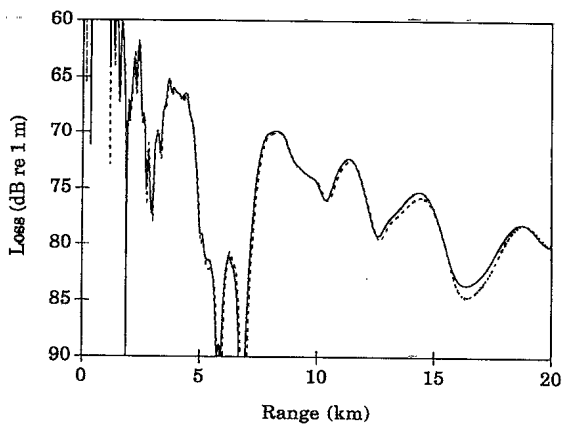

FIG. 3. Transmission loss versus range for the Bucker profile and a receiver depth of 90 m. Dashed line: SAFARI. Solid line: Hybrid split-step/finite-difference PE using a one-term Padé approximation to the density component of Q_1'.

wave number axis (see Ref. 12, pp. 249–251). To suppress reflections from the edge of the PE computational window, a linearly increasing attenuation is introduced between depths of $z=1024$ m and $z=2048$ m. A 100-Hz acoustic source is located at $z=30$ m. Reference solutions for this problem, computed for receivers at $z=90$ m and $z=240$ m, were obtained using the spectral integration model SAFARI.[26]

Before presenting our hybrid split-step/finite-difference results, we exhibit in Figs. 1 and 2, for the shallow and deep receiver respectively, traditional split-step PE calculations for the Bucker profile obtained by smoothing the density jump appearing in the operator $\tilde{Q}$ according to Eq. (9).[9,11] In our calculations, we employed a range step size of $\Delta r=10$ m, a depth step size of $\Delta z=2$ m, and a value of $c_0=1500$ m s^{-1}. Further, as mentioned in Ref. 12 (p. 385), it is necessary to multiply $\tilde{\psi}$ by $\sqrt{\rho}$ before computing transmission loss. For the recommended value of the smoothing parameter $k_0L=2$, the split-step PE produces reasonable results, although the transmission losses at ranges $r<5$ km lack the detailed structure evident in the reference solution. The quality of the PE results in Fig. 2 for the deep receiver is gratifying, considering that this depth is within the transition region of the smoothed density profile. It is worthwhile pointing out that PE codes based solely on finite-difference solvers can readily handle this problem. In fact, for the same values of Δr, Δz and c_0, the transmission loss curve obtained using the Claerbout approximation in Eq. (16) (not shown here) agrees with the SAFARI curve shown to within a linewidth at all ranges.

Next, we apply the hybrid procedures of the previous section to this test case. The PE calculations shown in Figs. 3 and 4 were obtained by combining a split-step evaluation of the γ-independent terms of Eq. (18) with a finite-difference solution for the γ-dependent term according to Eq. (27). It is seen that for both receiver depths, our hybrid approach both reproduces the detailed structure of the SAFARI result at ranges $r<5$ km and maintains satisfactory accuracy at longer ranges. The long-range behavior is not improved by incorporating the next higher-order operator Q_2', which suggests that the errors implicit in the operator splitting associated with Eq. (20) generates the major source of approximation error in our calculations. On the other hand, including the Q_2' higher-order terms greatly reduces

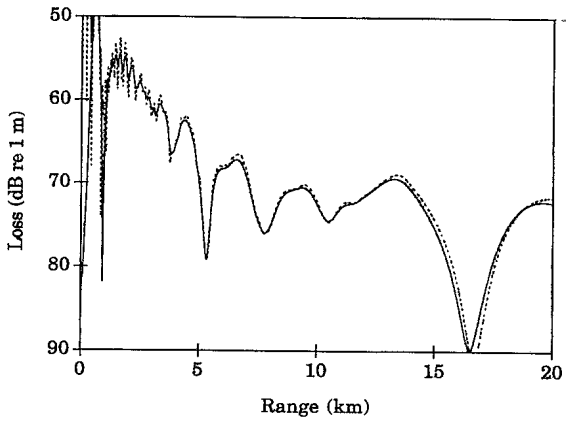

FIG. 2. Transmission loss versus range for the Bucker profile and a receiver depth of 240 m. Dashed line: SAFARI. Solid line: Split-step PE using $\tilde{Q}$ with $k_0L=2$.

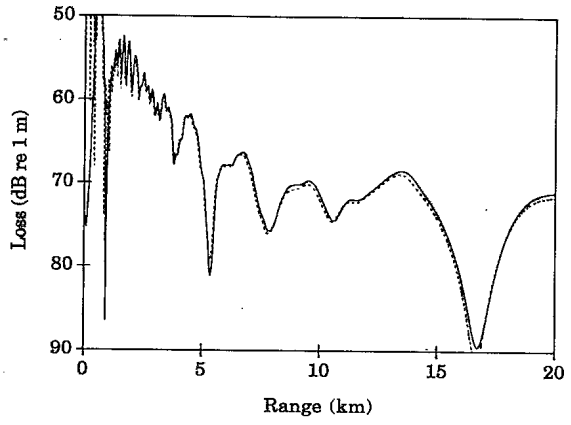

FIG. 4. Transmission loss versus range for the Bucker profile and a receiver depth of 240 m. Dashed line: SAFARI. Solid line: Hybrid split-step/finite-difference PE using a one-term Padé approximation to the density component of Q_1'.

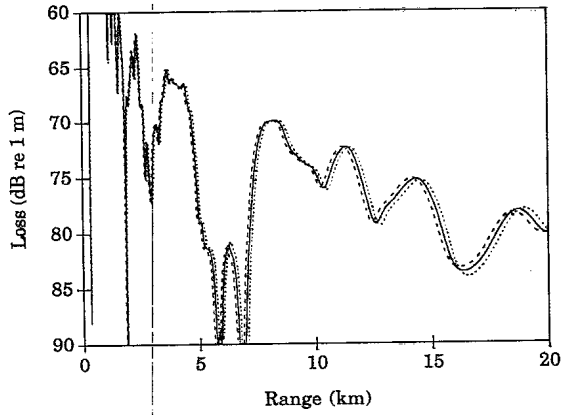

FIG. 5. Hybrid split-step/finite-difference PE predictions for the Bucker profile at a receiver depth of 90 m using a one-term Padé approximation to the density-dependent component of Q_1'. Dotted line: $c_0=1480$ m s^{-1}. Solid line: $c_0=1500$ m s^{-1}. Dashed line: $c_0=1520$ m s^{-1}.

the sensitivity of the hybrid procedure to variations in reference sound speed c_0. This feature is illustrated in Figs. 5 and 6, which show the variations in transmission losses at the shallow receiver depth for three values of c_0 for the hybrid procedure based on the operators Q_1' and Q_2', respectively. The dependence of the Q_1' solutions on c_0 shown in Fig. 5 is removed when the higher-order terms of Q_2' are included (all three transmission loss curves in Fig. 6 overlay one another). Note that such a behavior mirrors a similar decrease in sensitivity to c_0 in a previous model of a leaky surface duct[16] and would therefore be expected to extend to the smoothed density technique of Eq. (9) as well.

The geoacoustic profile for the second example, given in Table II, corresponds to the deep-end section of the lossy wedge test case introduced as one of the ASA range-dependent benchmark problems.[27] Jump discontinuities in sound speed, density and absorption occur along the sloping wedge interface, i.e., the line z (m)$=200-50r$ (km). The coordinates of the apex of the wedge are $z=0$ m and $r=4$ km. Additionally, an absorbing layer with linearly increasing attenuation is inserted between the depths $z=512$ m and

TABLE II. Deep-end geoacoustic profile for ASA wedge case.

Depth (m)	Sound speed (m s^{-1})	Density (g cm^{-3})	Attenuation dB λ^{-1}
0	1500	1.0	0.0
200	1500	1.0	0.0
200	1700	1.5	0.5
512	1700	1.5	0.5
1024	1700	1.5	5.0

$z=1024$ m.[6,28] A 25-Hz acoustic source, positioned at $z=100$ m, in the proximity of a node of the second lowest-order mode, excites both of the other propagating modes while the receivers are located at $z=30$ m and $z=150$ m.

The widespread practice of approximating a range-dependent waveguide by a sequence of range-independent sections and then marching the outgoing field according to a simple range-updating procedure is known to violate conservation of energy at the vertical interfaces between sections.[29] Although energy-conserving,[30] two-way,[31] and sloping[32,33] PEs have been introduced to ameliorate this problem, we will here apply standard one-way PE techniques with a range step size of $\Delta r=5$ m, a depth step size of $\Delta z=1$ m, and a value of $c_0=1500$ m s^{-1}. Reference solutions are calculated with a finite-difference PE based on a two-term Padé approximation for the operator Q_2.

The transmission losses for the split-step operator $\tilde{Q}$ and hybrid split-step/finite-difference operator Q_1' are shown in Figs. 7 to 10. For both receiver depths, the results obtained using the hybrid operator Q_1' [observing the order of the propagators in Eq. (18)] agree better with the reference curves generated using Q_2 than the results obtained with the traditional split-step approach based on $\tilde{Q}$. The smaller range shifts observed in the multipath interference structure in Figs. 8 and 10 further suggest that the hybrid PE formulation leads to a wider-angle capability than the traditional split-step PE.

Unfortunately, introducing successive higher-order terms in the operator Q_2' yields appreciable errors in comparison to the results shown in Figs. 8 and 10. Evidently, the

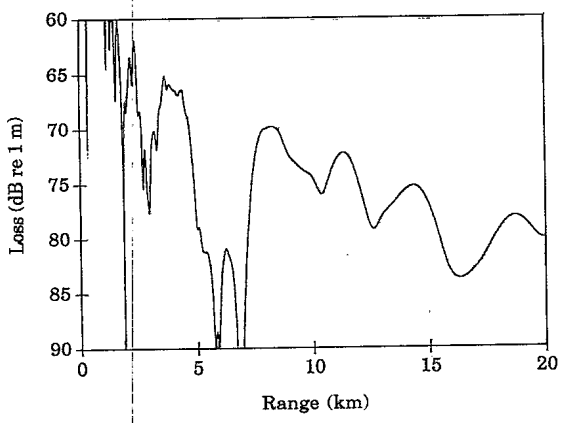

FIG. 6. Hybrid split-step/finite-difference PE predictions for the Bucker profile at a receiver depth of 90 m using one-term Padé approximations to the density-dependent components of Q_2'. Dotted line: $c_0=1480$ m s^{-1}. Solid line: $c_0=1500$ m s^{-1}. Dashed line: $c_0=1520$ m s^{-1}.

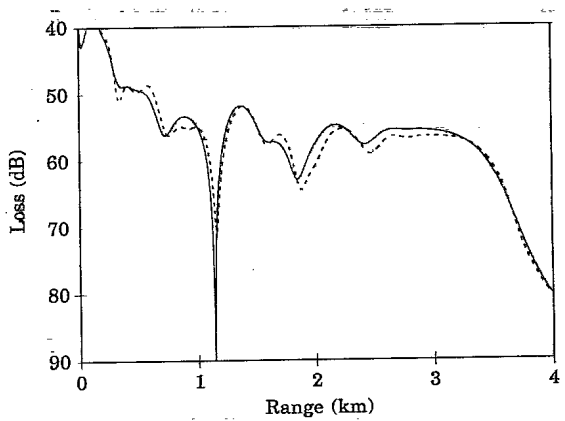

FIG. 7. Transmission loss versus range for the ASA wedge and a receiver depth of 30 m. Dashed line: Finite-difference PE using the two-term Padé approximation Q_2. Solid line: Split-step PE using $\tilde{Q}$ with $k_0L=2$.

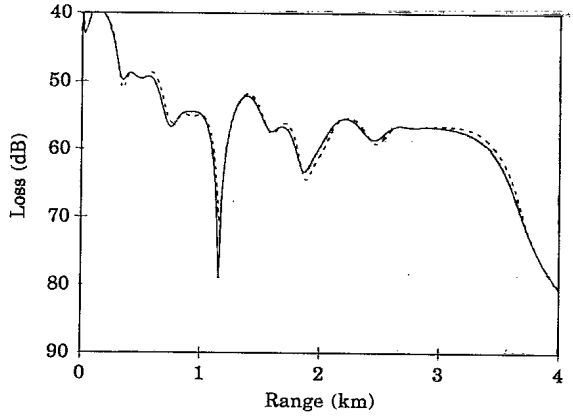

FIG. 8. Transmission loss versus range for the ASA wedge and a receiver depth of 30 m. Dashed line: Finite-difference PE using the two-term Padé approximation Q_2. Solid line: Hybrid split-step/finite-difference PE using a one-term Padé approximation to the density component of Q_1'.

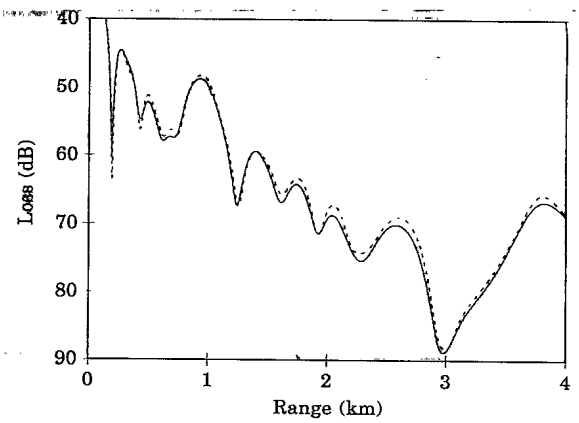

FIG. 10. Transmission loss versus range for the ASA wedge and a receiver depth of 150 m. Dashed line: Finite-difference PE using the two-term Padé approximation Q_2. Solid line: Hybrid split-step/finite-difference PE using a one-term Padé approximation to the density component of Q_1'.

correction terms of Eqs. (28)–(30) introduce significant high-frequency components into the acoustic field at the vicinity of the large sound speed discontinuity along the sea-bottom interface which cannot be adequately propagated by our operator approximation. Future research may, however, lead to a procedure for circumventing this difficulty. Similar effects are expected to appear as well in a related split-step approximation, recently introduced for acoustic thermometry applications.[34] As this formulation requires a non-linear transformation of the sound speed profile applicable to media in which the sound speed varies smoothly with depth, numerical difficulties are expected in shallow-water scenarios where realistic geoacoustic discontinuities must be incorporated. On the other hand, for sufficiently smooth profiles such as those of Ref. 34, both the transformation method and the procedure based on hybrid operator Q_2' should dramatically reduce the degree of sensitivity to the value of c_0 as demonstrated in Refs. 16 and 23 for both the leaky surface-duct and Bucker profiles.

Finally, regarding the computational efficiency of the hybrid split-step/finite-difference approach, the operator Q_1' requires solving a system of tridiagonal equations in addition to the multiplications and additions inherent in Eq. (21). As a result, the runtime for our scalar code is about 20% greater than that associated with the standard split-step PE for the examples presented above.

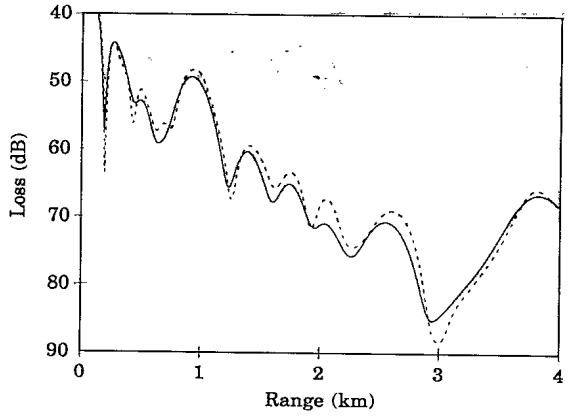

FIG. 9. Transmission loss versus range for the ASA wedge and a receiver depth of 150 m. Dashed line: Finite-difference PE using the two-term Padé approximation Q_2. Solid line: Split-step PE using $\tilde{Q}$ with $k_0L=2$.

IV. CONCLUSIONS

In this paper, we have advanced a hybrid split-step technique for modeling acoustic propagation in the presence of nonuniform density profiles. Our method separates the propagation operator into a product of the standard density-independent terms and a new density-dependent contribution which can be evaluated separately by finite-differencing. For the examples shown, the accuracy of the resulting method exceeds that of the standard procedure for including density variations into the split-step propagation technique. Moreover, because our algorithm does not rely on an empirically determined smoothing function, geoacoustic media that contain density jumps are incorporated in a natural way. Unfortunately, as a result of the additional operator splitting, some precision is necessarily sacrificed with respect to the standard full finite-difference technique. In wide-angle problems involving nearly constant sound-speed and density profiles, however, the increased accuracy afforded by the split-step approach should more than offset the error inherent in the operator splitting. Further, in such profiles, hybrid split-step/finite difference and split-step/Lanczos procedures can be employed to reduce significantly the reference sound-speed dependence of the results. We thus believe that the hybrid method introduced here provides a practical alternative to treating density variations in existing split-step codes, particularly for shallow-water applications.

ACKNOWLEDGMENTS

Financial support for one of us (DY) was provided through the scientific research Contract No. W7708–4–1214/01–XSA with the Defence Research Establishment Pacific (now Esquimalt Defence Research Detachment, a Division of the Defence Research Establishment Atlantic). The same author would like to acknowledge the National Re-

search Council of Canada, the Ontario Center for Materials Research, BNR and Corning Glass for continued funding.

[1] S. T. McDaniel and D. Lee, "A finite-difference treatment of interface conditions for the parabolic wave equation," J. Acoust. Soc. Am. **71**, 855–858 (1982).
[2] D. Lee and S. T. McDaniel, "Ocean acoustic propagation by finite-difference methods," Comput. Math. Appl. **14**, 305–423 (1987).
[3] A. R. Mitchell, *Computational Methods in Partial Differential Equations* (Wiley, New York, 1969), Chap. 2, pp. 22–32.
[4] K. R. Kelly, R. W. Ward, S. Treitel, and R. M. Alford, "Synthetic seismograms: a finite-difference approach," Geophysics **41**, 2–27 (1976).
[5] M. D. Collins, "Higher-order and elastic parabolic equations for wave propagation in the ocean," in *Computational Acoustics—Vol. 3*, edited by D. Lee, A. Cakmak, and R. Vichnevetsky (North-Holland, New York, 1990), pp. 167–184.
[6] D. J. Thomson, "Wide-angle parabolic equation solutions to two range-dependent benchmark problems," J. Acoust. Soc. Am. **87**, 1514–1520 (1990).
[7] P. G. Bergman, "The wave equation in a medium with a variable index of refraction," J. Acoust. Soc. Am. **17**, 329–333 (1946).
[8] L. M. Brekhovskikh, *Waves in Layered Media* (Academic, New York, 1980), 2nd ed., Chap. III, pp. 161–162.
[9] F. D. Tappert, "The parabolic approximation method," in *Wave Propagation and Underwater Acoustics*, edited by J. B. Keller and J. S. Papadakis (Springer-Verlag, New York, 1977), Chap. 5, pp. 224–287.
[10] F. D. Tappert and L. Nghiem-Phu, "Modeling of pulse response functions of bottom-interacting sound using the parabolic equation method," in *Ocean Seismo-Acoustics*, edited by T. Akal and J. M. Berkson (Plenum, New York, 1986), pp. 129–137.
[11] B. H. Maranda and D. J. Thomson, "A digital filter approach for treating density variations in the split-step algorithm of underwater acoustics," in *IEEE Pacific Rim Conference on Communications, Computers and Signal Processing, 4–5 June 1987, Victoria, BC, Conference Proceedings* (IEEE, New York, 1987), pp. 342–345.
[12] F. B. Jensen, W. A. Kuperman, M. B. Porter, and H. Schmidt, *Computational Ocean Acoustics* (AIP Press, New York, 1994), pp. 384–385.
[13] F. B. Jensen and M. G. Martinelli, "The SACLANTCEN parabolic equation model (PAREQ)," SACLANT Undersea Research Centre, La Spezia, Italy (1985).
[14] E. S. Holmes and L. A. Gainey, "The Navy Standard Parabolic Equation Model, Broadband PE, and PE Workshop II," in *PE Workshop II: Proceedings of the Second Parabolic Equation Workshop*, edited by S. A. Chin-Bing, D. B. King, J. A. Davis, and R. B. Evans (Naval Research Laboratory, US Government Printing Office, 1993), pp. 175–213.
[15] K. B. Smith and F. D. Tappert, "UMPE: The University of Miami Parabolic Equation Model, Version 1.0," Marine Physical Laboratory Tech. Memo. **432**, May 1993.
[16] D. Yevick and D. J. Thomson, "Split-step/finite-difference and split-step/Lanczos algorithms for solving alternative higher-order parabolic equations," J. Acoust. Soc. Am. **96**, 396–405 (1994).
[17] J. A. Davis, D. White, and R. C. Cavanagh, "NORDA Parabolic Equation Workshop, 31 March–3 April 1981," Tech. Note 143, Naval Ocean Research and Development Activity, NSTL Station, MS, 1982.
[18] J. F. Claerbout, "Coarse grid calculations of waves in inhomogeneous media with application to delineation of complicated seismic structure," Geophysics **35**, 407–418 (1970).
[19] M. D. Collins, "Benchmark calculations for higher-order parabolic equations," J. Acoust. Soc. Am. **87**, 1535–1538 (1990).
[20] M. D. Feit and J. A. Fleck, "Light propagation in graded-index optical fibers," Appl. Opt. **17**, 3990–3998 (1978).
[21] D. J. Thomson and N. R. Chapman, "A wide-angle split-step algorithm for the parabolic equation," J. Acoust. Soc. Am. **74**, 1848–1854 (1983).
[22] D. Yevick, J. Yu, W. Bardyszewski, and M. Glasner, "Stability issues in vector electric field propagation," Photon. Technol. Lett. **7**, 656–658 (1995).
[23] D. Yevick and B. Hermansson, "Convergence properties of wide-angle techniques," Photon. Technol. Lett. **6**, 1457–1460 (1994).
[24] F. D. Tappert and R. H. Hardin, "Computer simulation of long-range ocean acoustic propagation using the parabolic equation method," in *Proceedings of the 8th International Congress on Acoustics* (Goldcrest, London, 1974), Vol. 2, p. 452.
[25] B. Hermansson, D. Yevick, W. Bardyszewski, and M. Glasner, "The unitarity of split-operator finite difference and finite-element methods: Application to longitudinally varying semiconductor rib waveguides," IEEE J. Light. Technol. **7**, 1866–1874 (1990).
[26] H. Schmidt, "SAFARI Seismo-Acoustic Fast field Algorithm for Range-Independent environments," SACLANT Undersea Research Centre, San Bartolomeo, Italy, Rep. SR-113, 1988.
[27] F. B. Jensen and C. M. Ferla, "Numerical solutions of range-dependent benchmark problems in ocean acoustics," J. Acoust. Soc. Am. **87**, 1499–1510 (1990).
[28] D. Yevick, J. Yu, and Y. Yayon, "Optimal absorbing boundary conditions," J. Opt. Soc. Am. A **12**, 107–110 (1995).
[29] M. B. Porter, F. B. Jensen, and C. M. Ferla, "The problem of energy-conservation in one-way models," J. Acoust. Soc. Am. **89**, 1058–1067 (1991).
[30] M. D. Collins and E. K. Westwood, "A higher-order energy-conserving parabolic equation for range-dependent ocean depth, sound speed, and density," J. Acoust. Soc. Am. **89**, 1068–1075 (1991).
[31] M. D. Collins and R. B. Evans, "A two-way parabolic equation for acoustic backscattering in the ocean," J. Acoust. Soc. Am. **91**, 1357–1368 (1992).
[32] D. Lee and W. L. Siegmann, "Finite difference treatment of irregular interfaces: An error analysis," J. Comp. Acoust. **3**, 1–14 (1995).
[33] G. H. Brooke, D. J. Thomson, and P. M. Wort, "A sloping-boundary condition for efficient PE calculations in range-dependent acoustic media," J. Comp. Acoust. **4**, 11–27 (1996).
[34] F. D. Tappert, J. L. Spiesberger, and L. Boden, "New full-wave approximation for ocean acoustic travel time predictions," J. Acoust. Soc. Am. **97**, 2771–2782 (1995).

#502901